Modulation response of nanolasers: what rate equation approaches miss

Roland Aust, Thorben Kaul, Cun-Zheng Ning, Benjamin Lingnau & Kathy Lüdge

Optical and Quantum Electronics

ISSN 0306-8919
Volume 48
Number 2

Opt Quant Electron (2016) 48:1-8
DOI 10.1007/s11082-016-0378-4

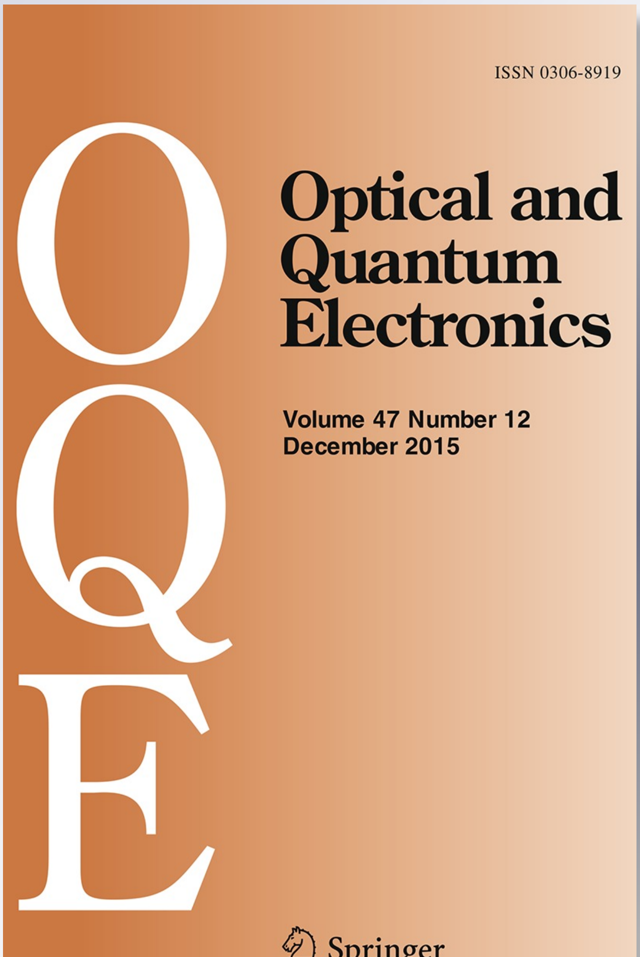

Springer

Opt Quant Electron (2016) 48:109
DOI 10.1007/s11082-016-0378-4

Modulation response of nanolasers: what rate equation approaches miss

Roland Aust[1] · Thorben Kaul[1] · Cun-Zheng Ning[2] · Benjamin Lingnau[1] · Kathy Lüdge[3]

Received: 2 October 2015 / Accepted: 6 January 2016

Abstract Rate equation approaches are a standard method to describe and examine the modulation dynamics of various semiconductor lasers, including nanolasers with high spontaneous emission rates. Using the more complex Bloch equation model we investigate the impact of the internal timescales on the stability and the modulation response. We demonstrate the limitation of rate equation approaches for systems where photon decay rate and polarization decay have similar orders of magnitude.

Keywords Nanolasers · Modulation · Spontaneous emission

1 Introduction

Decreasing the cavity volume of nanostructured semiconductor lasers entails a variety of consequences on the emission properties of the device, especially due to the increased rate of spontaneous emission (Li and Ning 2012; Zhang et al. 2014; Ning 2010; Neogi et al. 2002). Previous works on nanolaser devices already discussed how the Purcell-enhanced

This article is part of the Topical Collection on Numerical Simulation of Optoelectronic Devices, NUSOD' 15.

Guest edited by Julien Javaloyes, Weida Hu, Slawek Sujecki and Yuh-Renn Wu.

✉ Roland Aust
roland.aust@tu-berlin.de

1 Institut für Theoretische Physik, Technische Universität Berlin, Hardenbergstraße 36, 10623 Berlin, Germany

2 School of Electrical, Computer and Energy Engineering, Arizona State University, P.O. Box 875706, Tempe, AZ 85287-5706, USA

3 Freie Universität Berlin, Fachbereich Physik, Arnimallee 14, 14195 Berlin, Germany

Published online: 20 January 2016

spontaneous emission may increase the modulation bandwidth below threshold (Lau et al. 2009) or reduce it above threshold (Shore 2010) using rate equations. However, extensive microscopic modeling of the light emitting characteristics of nanolasers showed that care has to be taken, as rate equation results may underestimate the modulation properties (Lorke et al. 2013) and also may misinterpret the impact of the microscopic scattering processes (Lorke et al. 2010; Suhr et al. 2010). In the present paper we do not aim at quantitative description of nanolasers, as elaborated theories already exist (Chow et al. 2014), but we want to deepen the understanding of the interplay between the different timescales that are present in such a nanolaser device, especially investigating the effect of photon lifetime, polarization decay and spontaneous emission rate. Thus, by using a simplified microscopically-adapted Bloch-equation model, we analyze the impact of varying timescales on the dynamic response of the laser and discuss what rate equations miss for the case of similar photon and polarization decay. We also show that it is hard to predict the effect of spontaneous emission enhancement without exactly knowing the remaining timescales, as both a better and a decreased modulation bandwidth can result.

2 Modeling

We describe our quantum-dot nanolaser system by using the following Bloch equation model containing equations for the field amplitude E, the polarization p, and the inversion d. It is adapted from simple laser equations (Ning and Haken 1992) with additional Purcell-enhanced spontaneous emission rate (Lau et al. 2009) and microscopic details of quantum-dot laser dynamics (Lüdge 2012; Lingnau et al. 2012; Lüdge and Schöll 2009).

$$\dot{E} = -\kappa E + 2Z^{QD}\Gamma|g|p + \frac{Z^{QD}\Gamma\beta}{\tau_{\mathrm{eff}}E^*}\left(\frac{d+1}{2}\right)^2 \tag{1}$$

$$\dot{p} = -\gamma p + |g|Ed \tag{2}$$

$$\dot{d} = -4|g|Ep + \frac{d_0(w_e) - d}{T_1(w_e)} - \frac{1}{\tau_{\mathrm{eff}}}\left(\frac{d+1}{2}\right)^2 \tag{3}$$

The dominating timescales that will be varied are the polarization decay γ, the photon decay rate 2κ and the effective rate of spontaneous emission $\tau_{\mathrm{eff}} = \frac{\tau_{sp}}{F_P}$ given by the Purcell factor F_P and the spontaneous emission rate τ_{sp}. The spontaneous emission and coupling factors are indicated with β and $|g|$, respectively. Z^{QD} denotes the number of quantum dots in the active region. We chose those parameters to yield a gain of $G = 2Z^{QD}\Gamma\frac{g^2}{\gamma c_n} = 700\,\mathrm{cm}^{-1}$ with c_n as the speed of light in the laser medium. For simplicity we assume equal electron and hole carrier densities $\rho_e = \rho_h$ in the quantum dots, define the inversion as $d = \rho_e - \rho_h - 1$ and set $\beta = 1$. The carrier-carrier Coulomb scattering processes needed to fill the confined quantum-dot levels are modeled by the inversion lifetime $T_1(w_e) = (S^{in} + S^{out})^{-1}$ and the pump strength $d_0(w_e) = \frac{2S^{in}}{S^{in}+S^{out}} - 1$, where the scattering rates S^{in}, S^{out} (see Fig. 1c) are described in Lüdge (2012); Lingnau et al. (2012); Lüdge and Schöll (2009). In this simplified approach the carrier density in the surrounding quantum-well $w_{e/h}$ takes the role of the pump current. Figure 1b depicts that both, T_1 and d_0, increase with increasing quantum-well carrier density.

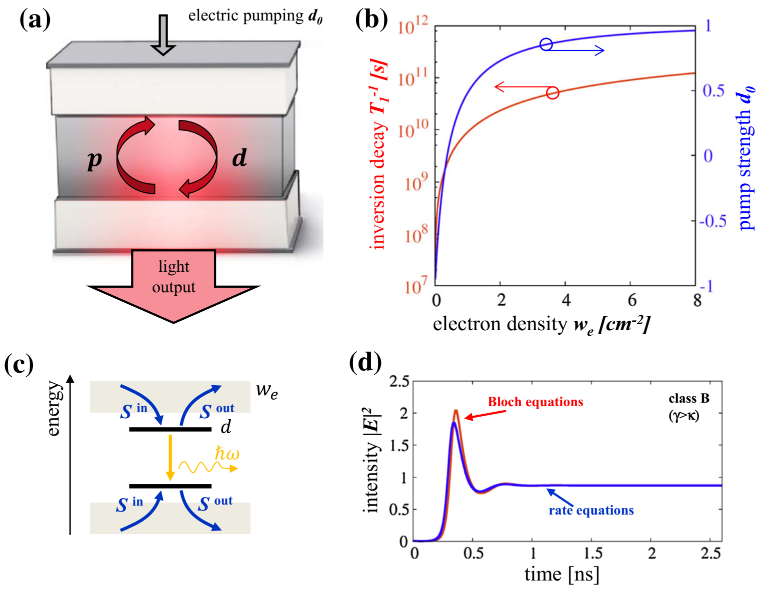

Fig. 1 **a** Quantum-dot nanolaser scheme, **b** inversion decay $T_1^{-1}(w_e)$ (*red line*) and pump strength $d_0(w_e)$ (*blue line*) in dependence of the wetting layer electron density w_e, **c** in and out scattering rate scheme, **d** class B laser ($T^{-1} < \kappa \ll \gamma$) time series for rate (*blue line*) and Bloch (*red line*) equations, parameters: $T^{-1} = 2 \times 10^9\ \mathrm{s}^{-1}$, $\kappa = 10^{10}\ \mathrm{s}^{-1}$, $\gamma = 2 \times 10^{11}\ \mathrm{s}^{-1}$. (Color figure online)

Eliminating the polarization dynamics of Eq. (2) adiabatically ($\dot{p} = 0$) (Ning and Haken 1992) and using the resulting static relation $p(E, d)$ within the two remaining equations leads us to the corresponding rate equation system.

$$\dot{E} = -\kappa E + \frac{2Z^{QD}\Gamma g^2}{\gamma} E d + \frac{Z^{QD}\Gamma\beta}{\tau_{\mathrm{eff}} E^*}\left(\frac{d+1}{2}\right)^2 \tag{4}$$

$$\dot{d} = -\frac{4g^2}{\gamma} E^2 d + \frac{d_0(w_e) - d}{T_1(w_e)} - \frac{1}{\tau_{\mathrm{eff}}}\left(\frac{d+1}{2}\right)^2 \tag{5}$$

For the case of fast polarization decay γ (class A or B laser Arecchi et al. (1984)) the expected results of both models are equal, which is shown exemplarily in Fig. 1d. However, deviations exist for the case of $\kappa \geq \gamma$, leading to large deviations in the modulation response. Following the terminology of laser classification, we introduce class C_A and class C_B lasers. Those are class C lasers ($\kappa \geq \gamma$) that do (C_B laser) or do not (C_A laser) show relaxation oscillations.

3 Results

Figure 2 characterizes the dynamics of a class C_A laser ($T^{-1} \approx \kappa \approx \gamma$) modeled by the Bloch equation system. The time series (Fig. 2c) show different behavior for increasing w_e (increases from top to bottom). For low pumping, regular intensity pulsations occur which

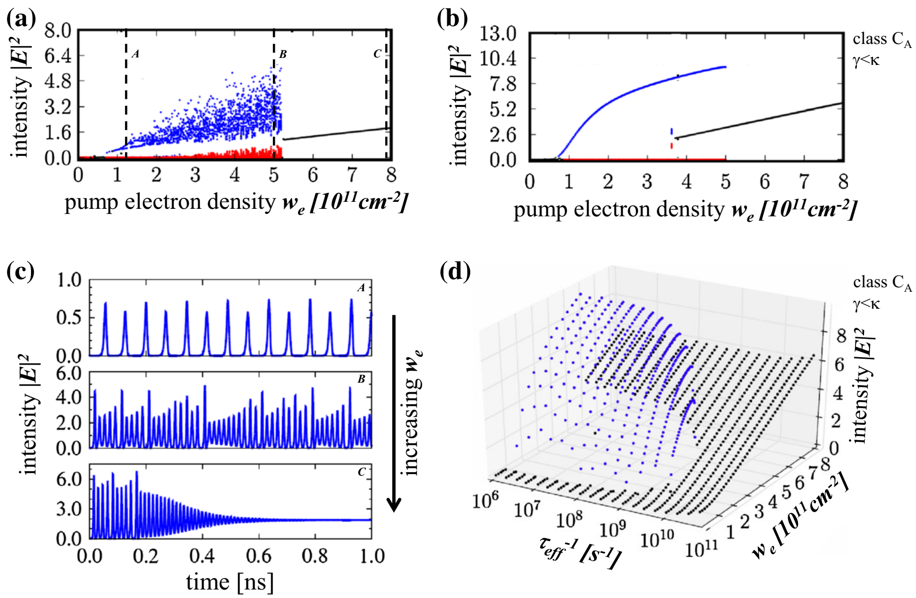

Fig. 2 **a**, **b** Bifurcation diagrams (intensity vs. carrier density w_e). *Blue* (*red*) *dots* correspond to intensity maxima (minima), *black dots* correspond to cw output. Parameters: **a** $\kappa = 3 \times 10^{11}\,\mathrm{s}^{-1}$, $\gamma = 10^{11}\,\mathrm{s}^{-1}$, **b** $\tau_{\mathrm{eff}}^{-1} = 10^{8}\,\mathrm{s}^{-1}$, $\kappa = 10^{11}\,\mathrm{s}^{-1}$, $\gamma = 10^{10}\,\mathrm{s}^{-1}$. **c** Class C_A laser Bloch equation time series for three different values of w_e (*upper panel A* $w_e = 1.2 \times 10^{11}\,\mathrm{cm}^{-2}$, *middle panel B* $w_e = 5 \times 10^{11}\,\mathrm{cm}^{-2}$, *lower panel C* $w_e = 8 \times 10^{11}\,\mathrm{cm}^{-2}$ correspond to *vertical dashed lines* in **a**). Parameters: see **a**. **d** Bifurcation diagram as in **b**, but with additional τ_{eff}^{-1}-dependence. *Blue dots* denote intensity pulsation maxima, *black dots* cw emission. (Color figure online)

can be suppressed by a higher pump rate. As seen in Fig. 2c(C), continuous wave output is achieved for high pump rates after transients have died out. The detailed dependence on w_e, i.e., the corresponding bifurcation diagram (without spontaneous emission) is shown in Fig. 2a. The case for fixed spontaneous emission decay is shown in Fig. 2b. For low values of w_e, intensity pulsations may occur and for $3.8 \times 10^{11}\,\mathrm{cm}^{-2} < w_e < 5 \times 10^{11}\,\mathrm{cm}^{-2}$ we even observe a bistable behavior where the laser may either pulsate or operate with cw emission, depending on the initial conditions. Above $w_e = 5 \times 10^{11}\,\mathrm{cm}^{-2}$, only stable cw emission is possible. With increasing τ_{eff}^{-1} (see Fig. 2d), the bistable regime and the intensity pulsations are weakened until the laser operates in cw mode for all values of w_e. Thus, a strong spontaneous emission stabilizes the laser output.

Since we aim at discussing the potential of these nanolasers for modulation applications, we restrict the parameter range in the following to cw operation (high w_e). Choosing proper device parameters for the fabrication of nanolasers, a wide range of possible quality factors Q can be achieved (Ding and Ning 2013) which directly leads to our choice of κ between $10^{11}\,\mathrm{s}^{-1}$ and $10^{12}\,\mathrm{s}^{-1}$. The gain G is kept fixed. Changes of γ are given by adjusting g. Figure 3 shows the small signal modulation dynamics of the laser, i.e., the laser response to a modulation of the pump current, comparing both modeling approaches. The deviation between the rate (red lines in Fig. 3) and the Bloch (blue lines) equation approach is obvious and can be explained with the resonance induced by excitation of (damped) Rabi-oscillations. For A and C_A lasers (Fig. 3a–c), the Bloch system shows a (local) maximum of the response in all sub-figures, whereas the rate equation system is strictly

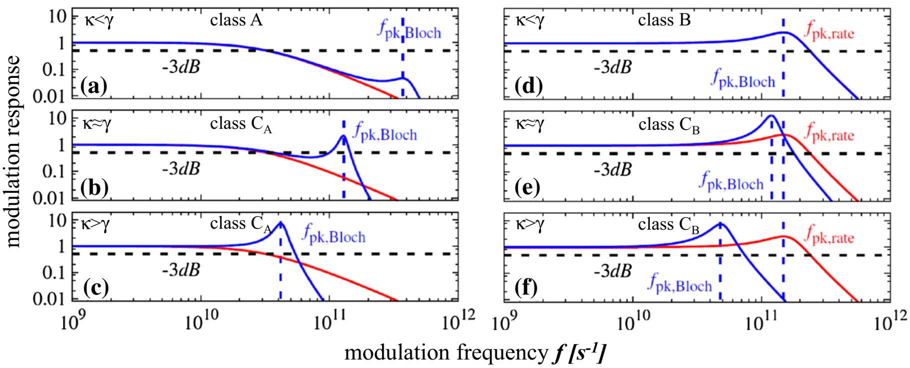

Fig. 3 Modulation response versus the current modulation frequency for rate (*red lines*) and Bloch (*blue lines*) equations. The resonance frequencies $f_{pk,rate}$ and $f_{pk,Bloch}$ are marked by *vertical dashed lines*. Parameters: $w_e = 8 \times 10^{11}\,\mathrm{cm}^{-2}$, $\tau_{\mathrm{eff}}^{-1} = 10^{10}\,\mathrm{s}^{-1}$; *left column* $\kappa = 10^{11}\,\mathrm{s}^{-1}$, *right column* $\kappa = 10^{12}\,\mathrm{s}^{-1}$; *a*, *d* $\gamma = 10^{12}\,\mathrm{s}^{-1}$; *b*, *e* $\gamma = 10^{11}\,\mathrm{s}^{-1}$; *c*, *f* $\gamma = 10^{10}\,\mathrm{s}^{-1}$. (Color figure online)

monotonically decreasing. For Fig. 3a $\gamma > \kappa$ holds, which leads to a resonance noticeably larger than the cutoff frequency $f_{-3\mathrm{dB}}$ and thus the cutoff frequencies of the rate equation approach do not differ from the Bloch equation system. When the polarization decay γ approaches the photon decay κ (see Fig. 3b, c) the modulation bandwidth of the Bloch system is noticeable improved by the additional resonance. However, with the chosen set of parameters, the response shortly drops below the threshold of -3 dB, before increasing again and forming the resonance peak at the frequency $f_{pk,Bloch}$. This cannot be modeled by the rate equation system due to its missing polarization dynamics. By choosing a higher photon decay, the early drop below -3 dB can be omitted (Fig. 3d–f. This choice of κ now yields the typical class B laser dynamics. Rate and Bloch equations show similar results (d) as long as $\gamma > \kappa$. When changing to lower values of the polarization decay γ (class C_B), the rate equation approach cannot predict the correct response of the nanolaser as seen in Fig. 3e, f. For the chosen value of τ_{eff}^{-1}, the cutoff frequencies of the class C_B laser is highly overestimated by the rate equation approach.

A more general view is given in Fig. 4a. In dependence on the reservoir carrier density w_e and the spontaneous emission decay τ_{eff}^{-1}, we show the modulation bandwidth for rate and Bloch equations for low (upper panels) and high (lower panels) κ (red color refers to hundreds of GHz). As long as $\gamma > \kappa$ holds, both approaches predict similar results, exemplarily shown by the rate equation results in the left column. However, for $\gamma \leq \kappa$ the spontaneous emission rate greatly influences the modulation bandwidth. Shaded areas mark the oscillatory dynamics given by the bifurcation diagrams in Fig. 2b, d. Keeping the result of Fig. 2d in mind, two competing effects have to be balanced, which leads to the existence of an optimal value of τ_{eff} (varies for different devices) to maximize $f_{-3\mathrm{dB}}$ (see Fig. 4b). For the typical photon lifetimes of $1ps$ ($\kappa = 1 \times 10^{12}\,\mathrm{s}^{-1}$) of nanolasers, large cutoff frequencies can be achieved by increasing the Purcell enhancement. As seen in Fig. 4b, $f_{-3\mathrm{dB}}$ of up to 350 GHz can be reached. However, we point out that the rate equation approach is not suitable for the prediction of $f_{-3\mathrm{dB}}$ in cases of C_A and C_B lasers. Depending on the spontaneous emission decay, it either over- or underestimates the bandwidth of the nanolaser.

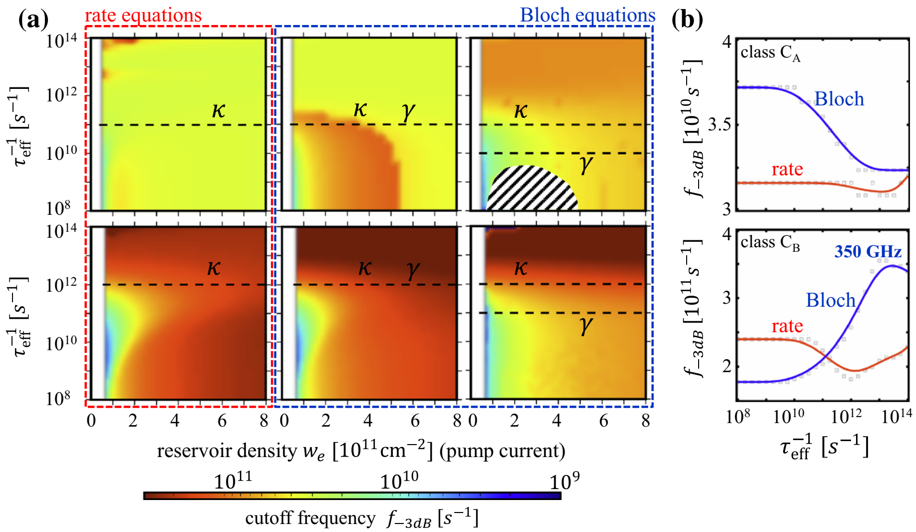

Fig. 4 **a** Cutoff frequency in dependence of the pump current and τ_{eff}^{-1}. Comparison of rate (*left panels*) and Bloch (*middle and right panels*) equations. *Upper panels* $\kappa = 10^{11}\,\mathrm{s}^{-1}$, *lower panels* $\kappa = 10^{12}\,\mathrm{s}^{-1}$. *Middle column* $\gamma = \kappa$, *right column* $\gamma < \kappa$. *Shaded areas* in *right panel* mark non-cw laser operation. **b** Cutoff frequency of rate (*red solid line*) and Bloch (*blue solid line*) equations in dependence of the spontaneous emission decay. Parameters as in *left and middle columns* of **a**, fixed $w_e = 8 \times 10^{11}\,\mathrm{cm}^{-2}$. (Color figure online)

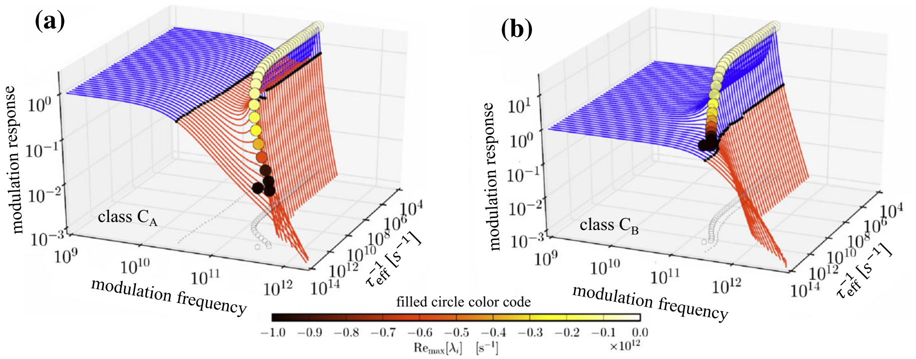

Fig. 5 Modulation response versus modulation frequency and spontaneous emission rates τ_{eff}^{-1} (Bloch equations). *Blue regions* represent responses above, *red regions* below $f_{-3\mathrm{dB}}$. *Filled circles* indicate the imaginary parts of the eigenvalues, *color* coded by the value of the real part. *White circles* and *gray dots* on the $\tau_{\mathrm{eff}}^{-1} - f_{mod}$−base plane are the projections of the imaginary part *circles* and the cutoff frequency *dots*. Parameters: $w_e = 8 \times 10^{11}\,\mathrm{cm}^{-2}$; **a** $\kappa = 10^{11}\,\mathrm{s}^{-1}$, $\gamma = 10^{11}\,\mathrm{s}^{-1}$, **b** $\kappa = 10^{12}\,\mathrm{s}^{-1}$, $\gamma = 10^{12}\,\mathrm{s}^{-1}$. (Color figure online)

Focusing on the Bloch equation system, Fig. 5 shows the complete modulation response curves of the Bloch system in dependence of the spontaneous emission rate τ_{eff}^{-1} for high pump current ($w_e = 8 \times 10^{11}\,\mathrm{cm}^{-2}$). Additionally, the eigenvalues of the linearized system are plotted. Their imaginary parts $\Im(\lambda_i)$ are marked by filled circles, color coded by the value of the largest real part $\Re(\lambda_i)$. In both sub-figures we recognize an increasing largest real part $\Re(\lambda_i)$ for higher spontaneous emission rates, which obviously weakens the resonance peaks. Fig. 5a shows situations similar to Fig. 3a–c (class C_A) while Fig. 5b presents the class C_B laser modulation response. It is obvious that, with increasing spontaneous emission rate, the cutoff frequency can be increased, which broadens the modulation bandwidth of the nanolaser device.

4 Conclusion

We investigate the effect of large variations in the spontaneous emission rate of a nanolaser on its stability and the modulation response. We show that rate equation models that are widely used to describe the modulation response of lasers may lead to wrong predictions for the case of nanolasers with equal polarization and photon decay rates. In those cases, the nanolaser dynamics cannot be predicted properly by rate equations. The stability of the examined nanolaser may be tuned by the choice of the active medium (dependence of γ), the cavity design (κ and τ_{eff}) or the pump current (d_0, T_1). Furthermore, we show that depending on the different internal timescales variations of the bandwidth can be expected. An optimal modulation response can be achieved by the proper choice of the device parameters: Nanolasers should be tuned to operate in the C_B regime where the interplay between Rabi oscillations and Purcell enhanced spontaneous emission can enhance the cutoff frequency up to 350 GHz.

Acknowledgments This work is supported by Deutsche Forschungsgemeinschaft in the framework of SFB 787, Project B2.

References

Arecchi, F.T., Lippi, G.L., Puccioni, G.P., Tredicce, J.R.: Deterministic chaos in laser with injected signal. Opt. Commun. **51**(5), 308–314 (1984)

Chow, W.W., Jahnke, F., Gies, C.: Emission properties of nanolasers during the transition to lasing. Light Sci. Appl. **3**, e201 (2014). doi:10.1038/lsa.2014.82

Ding, K., Ning, C.Z.: Fabrication challenges of electrical injection metallic cavity semiconductor nanolasers. Semicond. Sci. Technol. **28**(12), 124002 (2013). doi:10.1088/0268-1242/28/12/124002

Lau, E.K., Lakhani, A.A., Tucker, R.S., Wu, M.C.: Enhanced modulation bandwidth of nanocavity light emitting devices. Opt. Express **17**(10), 7790–7799 (2009). doi:10.1364/oe.17.007790

Li, D.B., Ning, C.Z.: Interplay of various loss mechanisms and ultimate size limit of a surface plasmon polariton semiconductor nanolaser. Opt. Express **20**(15), 16348–16357 (2012)

Lingnau, B., Lüdge, K., Chow, W.W., Schöll, E.: Influencing modulation properties of quantum-dot semiconductor lasers by carrier lifetime engineering. Appl. Phys. Lett. **101**(13), 131107 (2012)

Lorke, M., Nielsen, T.R., Mørk, J.: Influence of carrier dynamics on the modulation bandwidth of quantum-dot based nanocavity devices. Appl. Phys. Lett. **97**, 211106 (2010). doi:10.1063/1.3520525

Lorke, M., Suhr, T., Gregersen, N., Mørk, J.: Theory of nanolaser devices: rate equation analysis versus microscopic theory. Phys. Rev. B **87**, 205310 (2013)

Lüdge, K.: Modeling of quantum dot based laser devices. In: Lüdge, K. (ed.) Nonlinear Laser Dynamics—From Quantum Dots to Cryptography, chap. 1, pp. 3–34. Wiley, Weinheim (2012)

Lüdge, K., Schöll, E.: Quantum-dot lasers—desynchronized nonlinear dynamics of electrons and holes. IEEE J. Quantum Electron. **45**(11), 1396–1403 (2009)

Neogi, A., Lee, C.W., Everitt, H.O., Kuroda, T., Tackeuchi, A., Yablonovitch, E.: Enhancement of spontaneous recombination rate in a quantum well by resonant surface plasmon coupling. Phys. Rev. B **66**, 153305 (2002). doi:10.1103/physrevb.66.153305

Ning, C.Z.: Semiconductor nanolasers. Phys. Status Solidi (b) **247**(4), 774–778 (2010). doi:10.1002/pssb.200945436

Ning, C.Z., Haken, H.: Elimination of variables in simple laser equations. Appl. Phys. B **55**(2), 117–120 (1992). doi:10.1007/bf00324060

Shore, K.A.: Modulation bandwidth of metal-clad semiconductor nanolasers with cavity-enhanced spontaneous emission. Electron. Lett. **46**(25), 1688–1689 (2010). doi:10.1049/el.2010.2535

Suhr, T., Gregersen, N., Yvind, K., Mørk, J.: Modulation response of nanoLEDs and nanolasers exploiting Purcell enhanced spontaneous emission. Opt. Express **18**(11), 11230–11241 (2010). doi:10.1364/oe.18.011230

Zhang, Q., Li, G., Liu, X., Qian, F., Li, Y., Sum, T.C., Lieber, C.M., Xiong, Q.: A room temperature low-threshold ultraviolet plasmonic nanolaser. Nat. Commun. **5**, 4953 (2014). doi:10.1038/ncomms5953